Resonance Effects in Photoemission Time Delays

M. Sabbar,[1,*] S. Heuser,[1] R. Boge,[1] M. Lucchini,[1] T. Carette,[3,4] E. Lindroth,[4] L. Gallmann,[1,2] C. Cirelli,[1,†] and U. Keller[1]
[1]Physics Department, ETH Zurich, 8093 Zurich, Switzerland
[2]Institute of Applied Physics, University of Bern, 3012 Bern, Switzerland
[3]Laboratoire de Chimie Quantique et Photophysique, CP160/09, Université Libre de Bruxelles, B 1050 Brussels, Belgium
[4]Physics Department, Stockholm University, AlbaNova University Center, SE-106 91 Stockholm, Sweden
(Received 18 February 2015; published 23 September 2015)

We present measurements of single-photon ionization time delays between the outermost valence electrons of argon and neon using a coincidence detection technique that allows for the simultaneous measurement of both species under identical conditions. The analysis of the measured traces reveals energy-dependent time delays of a few tens of attoseconds with high energy resolution. In contrast to photoelectrons ejected through tunneling, single-photon ionization can be well described in the framework of Wigner time delays. Accordingly, the overall trend of our data is reproduced by recent Wigner time delay calculations. However, besides the general trend we observe resonance features occurring at specific photon energies. These features have been qualitatively reproduced and identified by a calculation using the multiconfigurational Hartree-Fock method, including the influence of doubly excited states and ionization thresholds.

DOI: 10.1103/PhysRevLett.115.133001 PACS numbers: 32.80.Fb, 32.80.Rm, 42.50.Hz

Recent measurements have demonstrated the possibility of probing single-photon ionization time delays of electrons originating from different initial states [1,2]. These pioneering measurements have triggered a great deal of theoretical studies in which the origin and interpretation has been debated controversially [1–8]. Currently, the most widely accepted understanding is that the measured time delay is composed of two different contributions: a measurement-induced delay that can be subtracted using computational results and the actual atom-specific ionization delay identified as the Wigner time delay [9,10].

The Wigner time delay is a measure for the spectral variation of the scattering phase. Scattering theories apply well to the mechanism of single-photon ionization because this process can be seen as a half-scattering event: after the electron is promoted from a bound state into the continuum, the electron scatters off the attractive Coulomb potential of the ion. The Wigner time delay τ_W is calculated as the energy derivative of the scattering phase φ_W which an electron wave packet acquires while propagating through the potential. Since the scattering phase is defined with respect to the free particle case, this particular delay definition represents the group delay of the wave packet referenced to the motion of the free particle with the same kinetic energy: $\tau_W \doteq \partial\varphi_W/\partial\omega = \hbar\partial\varphi_W/\partial E$. Because of this free-particle reference, the Wigner delay only considers delays that stem purely from the interaction of the electron with the potential.

However, our earlier experiments on ionization time delays in the tunneling regime have shown that the Wigner delay is not always an adequate concept [11,12]. Following the peak of the wave packet with the group delay (or Wigner delay) for tunneling is particularly problematic: first, it is not clear when the tunneling should exactly start and second, the energy-dependent transmission will reshape the wave packet such that the peak has no meaning for the tunneling time. In contrast to a light pulse, an electron wave packet disperses even in vacuum. Since the propagation of the peak of the wave packet is defined by the group delay, arbitrary group delays can be measured during propagation in combination with an appropriate energy-dependent transmission filter. The main difference between single-photon and tunnel ionization can be explained with a simplified picture of a wave packet propagating through a square potential exploring different regimes: $E < E_b$ for tunnel ionization and $E > E_b$ for single-photon ionization (Fig. 1). The tunnel barrier exhibits an energy-dependent high-pass transmission filter [Fig. 1(a)]. Figure 1(b) represents the case of a wave packet before and after the potential barrier with a kinetic energy $E < E_b$. For energies $E < E_b$ transmission is much more likely on the high-energy side of the wave packet. Through its selective transmission, this filter considerably reshapes the wave packet. This leads to the formation of a new peak of the wave packet that will not correctly describe the tunneling time as recently shown experimentally with the attoclock technique [11,12]. On the other hand, if the electron wave packet propagates with a kinetic energy sufficiently larger than the barrier height [Fig. 1(c)], the energy dependence of the amplitude filter can be neglected because the transmission probability is close to one for all the energies within the bandwidth of the wave packet (the modulations after the point $E = E_b$ shown in Fig. 1(a) are due to the reflected waves at the well boundary).

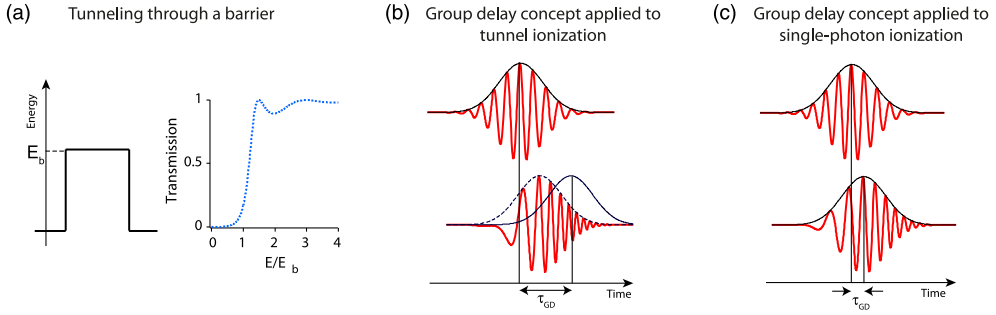

FIG. 1 (color online). Propagation of a wave packet through a square potential barrier. (a) Potential barrier of height E_b (black solid line) and transmission probability (blue dotted line) as a function of the ratio between the kinetic energy of the wave packet E and the barrier height E_b. (b) If the average kinetic energy of the wave packet is smaller than the barrier height, propagation involves tunneling. After propagation through the barrier, the wave packet disperses and its peak would be found at a time given by the dashed line. However, the transmission probability, shown in (a) acts as an energy-dependent high-pass filter (blue dotted line), inducing an additional temporal shift [solid line in lower part of panel (b)], which is not related to the time spent within the barrier but rather only depends on the specific shapes of filter and wave packet. (c) The situation where the energy of the wave packet is significantly larger than E_b resembles the situation after absorption of one photon leading to ionization; in this case the group delay is a direct measure of the propagation time of the wave packet because the energy dependence of the filter can be neglected in that regime. Therefore, a meaningful relation between the wave packet peaks before and after the filter persists.

In contrast to the tunneling regime, the Wigner delay is therefore expected to be a good concept to estimate single-photon ionization time delays, as has already been proposed theoretically [1–4,13] and demonstrated in experiments [1,2,14–16].

In this Letter, we present experimental results that allow the extraction of the photoionization time delay difference between the valence electrons of Ar ($3p$) and Ne ($2p$) with unsurpassed precision. We demonstrate that whenever a sharp resonance occurs, the simple picture of interpreting the *averaged* group delay (equivalent to an *averaged* Wigner delay) as photoionization time delay is not valid anymore. In analogy with the tunneling case [Fig. 1(b)] sharp resonances may act as an energy filter reshaping the electron wave packet, thus breaking the link between the peaks of the incoming and outgoing wave packets.

The novel experimental scheme applied here combines the attosecond streaking technique [17] with coincidence detection [18,19]. The unique ability to assign electrons to their parent ions allows us to simultaneously record multiple photoelectron spectra originating from different species even when the kinetic energies overlap. This capability and the careful treatment of the chirp of the attosecond pulse (attochirp) [20], allows us to extract the one-photon delay difference between Ar and Ne wave packets. The general trend of our results shows good agreement with Wigner delay calculation performed with the random phase approximation with exchange (RPAE) for energies between 28 and 35 eV. However, we also observe strong deviations at specific photon energies. These structures are qualitatively reproduced by single-channel scattering theory, when many electron correlation effects in Ar such as doubly excited states and ionization thresholds are accounted for [21].

The technique used to conduct the experiment is based on a reaction microscope, also known as a cold target recoil ion momentum spectroscopy (COLTRIMS) detector [18,19], in combination with a gas target containing a mixture of both species [22]. The gas mixture is ionized with single attosecond pulses (SAPs) of 12 eV bandwidth centered at a photon energy of about 35 eV. A moderately strong (about 3×10^{12} W/cm^2) infrared (IR) pulse with controllable delay modulates the final photoelectron momenta by streaking the freed electrons. The SAPs are generated with the polarization gating technique [23,24] using waveform controlled few-cycle IR laser pulses at a center wavelength of 735 nm and with a pulse duration of approximately 6 fs focused into an Ar gas target. The XUV-pump beam is first recombined with the delayed IR-probe through a holey mirror. Both beams are then collinearly focused by a toroidal mirror into the COLTRIMS detector, where ions and electrons are separated by a uniform dc electric field and guided towards space- and time-sensitive detectors. This allows for retrieving the full momentum vector—and therefore the kinetic energy—of each individual particle at the moment of ionization. Thus, applying a filter to the time-of-flight of the parent ions and to the momentum sum of ions and electrons allows for coincidence detection.

Based on attosecond streaking in coincidence we have been able to distinguish between electrons generated from Ar and Ne even though they energetically overlap. Figure 2(a) shows streaking traces simultaneously recorded for each species. In our analysis we only consider electrons emitted into a cone with an opining angle of 20° with respect to the XUV polarization axis. This procedure on the one hand reduces the overall counts in the spectrograms but on the other hand greatly avoids the effect of angularly dependent

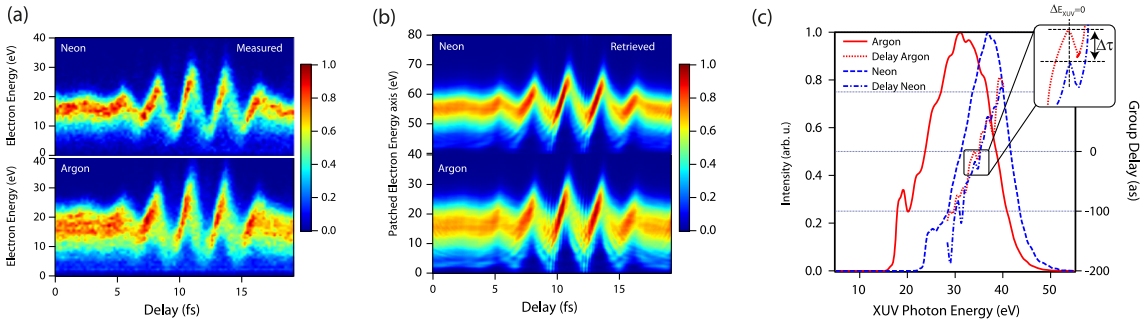

FIG. 2 (color online). Measured (a) and reconstructed (b) spectrograms for Ne and Ar photoelectrons collected within a cone of only 20° with respect to the XUV polarization axis; before applying the retrieval algorithm the two traces are patched together onto a common energy axis in order to ensure consistency in the reconstruction (see main text). (c) XUV spectra (solid and dashed lines) and group delays (dotted and dash-dotted lines) for Ar (red, solid and dotted) and Ne (blue, dashed and dash-dotted) computed by adding the ionization energy of the two targets to the spectra and group delays of the photoelectron wave packets retrieved with the FROG-CRAB algorithm. The inset in the top right shows the group delay difference $\Delta\tau$ calculated for electrons ionized by photons of the same XUV photon energy: this procedure ensures that the attochirp contribution to the photoemission time delay is removed.

time delays [25]. The energy-dependent phase of the photoelectron wave packet has been retrieved directly from the streaking traces by using an iterative algorithm known as frequency-resolved optical gating for complete reconstruction of attosecond bursts (FROG-CRAB) [26,27].

The algorithm has been fed with a matrix where both, the Ar and the Ne trace, had been patched together as illustrated in Fig. 2. This procedure ensures that the same IR vector potential and the same time zero are used for the reconstruction of the electron phase of both Ar and Ne. The resulting spectra and group delays are shown in Fig. 2(c). For both target atoms the group delay curve exhibits a large slope, on the order of 25 as/eV, indicating that the XUV pulse has a relatively strong attochirp. This means that XUV photons of different energy ionize the target atoms at different times. If we compared the group delays for Ar and Ne electron wave packets at the same kinetic energy, an apparent delay would arise caused by the different starting time of electrons of different energies. However, we can cancel the attochirp contribution to the photoemission time delay by evaluating the group delay difference between Ar and Ne, $\Delta\tau^{\mathrm{Ar/Ne}}$, at the same XUV photon energy as shown in Fig. 2(c).

The difference between the group delays, calculated for every XUV energy within a range where the spectral intensity of Ar and Ne spectra overlaps (between 28 and 40 eV) results in the energy-dependent group delay curve presented in Fig. 3(a) as green open circles. The data represent the averaged delays of 33 independently measured traces, while the error bars represent the standard deviation between the different data sets.

Recent advancements in computational methods for solving the time-dependent Schrödinger equation (TDSE) [4,28] have allowed for a more accurate description of the time-dependent photoionization process. Solving the TDSE in the single-active electron approximation demonstrated that the delay extracted from attosecond streaking experiments is identical with the Wigner time delay τ_{W} only in the case of a short-range model potential [4]. More generally, the presence of a Coulomb potential introduces an additive time delay, τ_{CLC} (Coulomb-laser coupling), which originates from the interaction of the streaking field with the long-range asymptotic tail of the Coulomb potential:

$$\tau_{\mathrm{streaking}} = \tau_{\mathrm{W}} + \tau_{\mathrm{CLC}}.$$

The measurement-induced contribution τ_{CLC} can be extracted from numerical calculations by computing the difference between the delays determined for a short-range and a Coulomb potential. It has been shown that this contribution is, to a great extent, universal, depending only on the net ion charge, the final electron energy, and the central frequency of the streaking field [3,28]. It is worth emphasizing that, to leading order, the calculated τ_{CLC} has no dependence on the IR intensity [4].

In order to understand the mechanism responsible for the observed time delays, we have compared our data to computational results. In a first approach we have taken the calculated Wigner delays for Ar and Ne from Ref. [7] which uses RPAE and thereby takes care of a large fraction of the many-electron correlation. In our analysis we considered only the $3p \rightarrow Ed$ channel for Ar and the $2p \rightarrow Ed$ channel for Ne, respectively, because ionization from a $3s$ (for Ar) or $2s$ (for Ne) shell is much weaker in the photon energy range considered in this work [7,29–31]. Furthermore, we neglected the contribution of channels leading to s-like states ($2p \rightarrow Es$ in Ne and $3p \rightarrow Es$ in Ar), in accordance with the Fano propensity rule [32]. For the case of Ar the validity of this assumption has been confirmed in a recent work [16], where it is demonstrated that the $3p \rightarrow Es$ channel has little influence on the measured delay in the energy range considered here. The laser-induced contribution (τ_{CLC}) to the delays has been calculated in Ref. [28] and can be removed from the

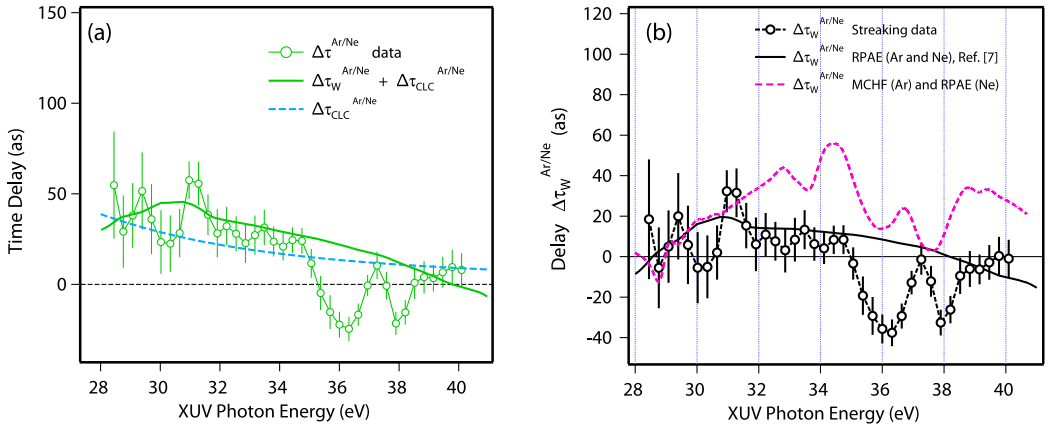

FIG. 3 (color online). (a) The measured streaking group delay difference between Ar and Ne electrons (green open circles connected by a solid line) is compared with the theoretical prediction (green solid line). The green solid line represents the sum of the calculated Wigner delay difference of Ar and Ne [7] and the corresponding measurement-induced delay difference [28], shown as a light blue dashed curve. (b) The black open circles connected by a dashed line represent the averaged group delay difference of the 33 independent measurements obtained after subtracting the laser-induced contribution $\Delta\tau_{\mathrm{CLC}}$ shown in (a). The black solid and the magenta dashed lines represent theory curves. The black solid line is computed by using one-photon matrix elements within the RPAE [7] both for Ar and Ne electrons. The magenta dashed line has been obtained by using MCHF [21] for Ar taking into account resonances and RPAE [7] for Ne.

data. Subtracting τ_{CLC} from the experimental data [presented as green circles in Fig. 3(a)], we finally obtain the difference between the Wigner delays of Ar and Ne as shown in Fig. 3(b) (black open circles). In the energy region between 28 and 35 eV, our data confirm the calculated Wigner time delays of Ref. [7] within the accuracy of the experiment.

However, in the energy range between 35 and 39 eV the deviation of the data from the theory is substantial. As we will show, a novel *ab initio* method, based on the multiconfigurational Hartree-Fock method (MCHF) [21] suggests that these sharp features are due to multiple resonances originating from shake-up thresholds in Ar opening within this energy range. Like RPAE, MCHF includes contributions from different angular channels, but can also account for the influence of doubly excited states and ionization thresholds that lead to multiple resonance structures. It is known that the Ar^+ level structure is particularly rich in the energy range between 35 and 39 eV and first theoretical evidence has been brought that the presence of resonances decaying into Ar^+ ($3s^2 3p^5$) and Ar^+ ($3s3p^6$) may greatly affect the measured one-photon delay [21,33]. We calculated the one-photon Wigner delay for Ar with MCHF for an outgoing d-wave and subtracted the one-photon Wigner delay for Ne estimated with RPAE. The latter is expected to be accurate due to the absence of resonances in the Ne^+ spectrum in the considered energy range. The Ar atomic structure model used here is described in more details in Appendix A of Ref. [21]. The Wigner delays computed with this model are obtained from photoelectron amplitudes convoluted by a Gaussian IR pulse with a full width at half maximum of 0.4 eV.

The result of this computation is shown in Fig. 3(b) as a magenta dashed line. Its discrepancy to the experimental data can partly be attributed to an inaccurate description of the $3p$ ionization Cooper minimum in Ar. Indeed, the Cooper minimum at about 50 eV accelerates $3p$ photoelectrons by several tens of attoseconds in a broad range of energies, including the range of interest [34]. The Cooper minimum in the MCHF simulations is too high and narrow, which leads to overestimations of the delays below 40 eV as large as up to 15 as.

More relevant to our discussion is the qualitative agreement between theory and the experimental data in the energy range between 35 and 39 eV which demonstrates the relevance of the atomic resonances for the determination of photoionization time delays. The idea that resonances could affect the measured time delays has earlier been raised in theoretical studies [35,36] and it has been investigated if this could be the key to understanding the hitherto unexplained magnitude of the delay in Ne in Ref. [1]. However, this explanation was ruled out due to the narrow nature of the expected resonances. With the energy-resolved results obtained here, on the other hand, the resonance effects are seen directly in the data.

Photoionization in the region from 33.5 to 35 eV exhibits a large number of resonances [37]. Following the calculations, the first group of resonances results from two $3p^4 nl$ $^2\mathrm{D}^e$ thresholds, at about 34.3 eV, and the second results from a $^2S^e$ threshold, at 36.5 eV. Future theoretical investigations are expected to confirm the attribution of the structure seen in the experimental time delays, since the presence of resonances can affect measured delays beyond their effect on the single-photon spectrum [33] which has

been applied here. Furthermore, inclusion also of the weak channel (leading to an outgoing *s*-electron) and the experimental angular integration might impact the results, particularly close to resonances where the relative channel amplitudes change rapidly.

A recent experiment has reported on photoionization time delays from different noble gases for a photon energy range similar to those presented here [16]. These results, obtained with a different technique based on an active delay stabilization scheme, show the same trend as in Fig. 3(b).

In conclusion, we have accessed photoionization time delays between valence electrons of two different atomic species by taking advantage of the unique capabilities of a COLTRIMS detector and the attosecond streaking technique. The time delays retrieved by our measurements confirm the general trend observed in theoretical studies that neglect a larger portion of many electron correlation effects in Ar. However, our experimental results exhibit features which we were able to attribute to the influence of resonances on photoionization time delays.

The authors thank M. Dahlström, R. Pazourek, S. Nagele, and H. J. Wörner for fruitful discussions. This work was supported by the ERC advanced Grant No. ERC-2012-ADG_20120216 within the seventh framework program of the European Union and by the NCCR MUST, funded by the Swiss National Science Foundation. M. L. acknowledges support from the ETH Zurich Postdoctoral Fellowship Program. T. C. acknowledges support from the IUAP - Belgian State Science Policy (BriX network P7/12). E. L. acknowledges support from the Swedish Research Council, Grant No. 2012-3668, and from the Wenner-Gren Foundation.

*msabbar@phys.ethz.ch
†cirelli@phys.ethz.ch

[1] M. Schultze *et al.*, Science **328**, 1658 (2010).
[2] K. Klünder *et al.*, Phys. Rev. Lett. **106**, 143002 (2011).
[3] J. M. Dahlström, A. L'Huillier, and A. Maquet, J. Phys. B **45**, 183001 (2012).
[4] S. Nagele, R. Pazourek, J. Feist, K. Doblhoff-Dier, C. Lemell, K. Tőkési, and J. Burgdörfer, J. Phys. B **44**, 081001 (2011).
[5] C.-H. Zhang and U. Thumm, Phys. Rev. A **84**, 033401 (2011).
[6] A. S. Kheifets and I. A. Ivanov, Phys. Rev. Lett. **105**, 233002 (2010).
[7] A. S. Kheifets, Phys. Rev. A **87**, 063404 (2013).
[8] J. M. Dahlström, T. Carette, and E. Lindroth, Phys. Rev. A **86**, 061402 (2012).
[9] E. P. Wigner, Phys. Rev. **98**, 145 (1955).
[10] F. T. Smith, Phys. Rev. **118**, 349 (1960).
[11] A. S. Landsman and U. Keller, Phys. Rep. **547**, 1 (2015).
[12] A. S. Landsman, M. Weger, J. Maurer, R. Boge, A. Ludwig, S. Heuser, C. Cirelli, L. Gallmann, and U. Keller, Optica **1**, 343 (2014).
[13] J. M. Dahlström, D. Guénot, K. Klünder, M. Gisselbrecht, J. Mauritsson, A. L'Huillier, A. Maquet, and R. Taïeb, Chem. Phys. **414**, 53 (2013).
[14] D. Guénot *et al.*, Phys. Rev. A **85**, 053424 (2012).
[15] C. Palatchi, J. M. Dahlström, A. S. Kheifets, I. A. Ivanov, D. M. Canaday, P. Agostini, and L. F. DiMauro, J. Phys. B **47**, 245003 (2014).
[16] D. Guénot *et al.*, J. Phys. B **47**, 245602 (2014).
[17] R. Kienberger *et al.*, Nature (London) **427**, 817 (2004).
[18] R. Dörner, V. Mergel, O. Jagutzki, L. Spielberger, J. Ullrich, R. Moshammer, and H. Schmidt-Böcking, Phys. Rep. **330**, 95 (2000).
[19] J. Ullrich, R. Moshammer, A. Dorn, R Dörner, L. Ph. H. Schmidt, and H. Schmidt-Böcking, Rep. Prog. Phys. **66**, 1463 (2003).
[20] Y. Mairesse *et al.*, Science **302**, 1540 (2003).
[21] T. Carette, J. M. Dahlstrom, L. Argenti,and E. Lindroth, Phys. Rev. A **87**, 023420 (2013).
[22] M. Sabbar, S. Heuser, R. Boge, M. Lucchini, L. Gallmann, C. Cirelli, and U. Keller, Rev. Sci. Instrum. **85**, 103113 (2014).
[23] I. J. Sola *et al.*, Nat. Phys. **2**, 319 (2006).
[24] G. Sansone *et al.*, Science **314**, 443 (2006).
[25] S. Heuser *et al.*, arXiv:1503.08966.
[26] Y. Mairesse and F. Quéré, Phys. Rev. A **71**, 011401 (2005).
[27] J. Gagnon and V. S. Yakovlev, Opt. Express **17**, 17678 (2009).
[28] R. Pazourek, S. Nagele, and J. Burgdörfer, Faraday Discuss. **163**, 353 (2013).
[29] B. Möbus, B. Magel, K.-H. Schartner, B. Langer, U. Becker, M. Wildberger, and H. Schmoranzer, Phys. Rev. A **47**, 3888 (1993).
[30] J. A. R. Samson and W. C. Stolte, J. Electron Spectrosc. Relat. Phenom. **123**, 265 (2002).
[31] J. M. Bizau and F. J. Wuilleumier, J. Electron Spectrosc. Relat. Phenom. **71**, 205 (1995).
[32] U. Fano, Phys. Rev. A **32**, 617 (1985).
[33] A. Jiménez-Galán, L. Argenti, and F. Martin, Phys. Rev. Lett. **113**, 263001 (2014).
[34] S. B. Schoun, R. Chirla, J. Wheeler, C. Roedig, P. Agostini, L. F. DiMauro, K. J. Schafer, and M. B. Gaarde, Phys. Rev. Lett. **112**, 153001 (2014).
[35] Y. Komninos, T. Mercouris, and C. A. Nicolaides, Phys. Rev. A **83**, 022501 (2011).
[36] J. Feist, O. Zatsarinny, S. Nagele, R. Pazourek, J. Burgdörfer, X. Guan, K. Bartschat, and B. I. Schneider, Phys. Rev. A **89**, 033417 (2014).
[37] H. W. van der Hart and C. H. Greene, Phys. Rev. A **58**, 2097 (1998).